7-20-1992

Planar H_2O Masers in Star-Forming Regions

Moshe Elitzur
University of Kentucky, moshe@pa.uky.edu

David J. Hollenbach
NASA/Ames Research Center

Christopher F. McKee
University of California - Berkeley

Planar H_2O Masers in Star-Forming Regions

Digital Object Identifier (DOI)
http://dx.doi.org/10.1086/171574

THE ASTROPHYSICAL JOURNAL, 394:221–227, 1992 July 20

PLANAR H_2O MASERS IN STAR-FORMING REGIONS

MOSHE ELITZUR,[1,2,3] DAVID J. HOLLENBACH,[2] AND CHRISTOPHER F. MCKEE[4]

Received 1991 July 9; accepted 1992 January 24

ABSTRACT

The planar geometry of shocked material is the key property in enabling the high brightness temperatures of H_2O masers in star-forming regions. We solve for the brightness temperature, the beaming angle, and the maser spot size for thin, saturated planar masers under the assumption that the velocity change across the maser due to ordered motions is small compared with the thermal or microturbulent line width. For a given set of physical parameters, the brightness temperature is essentially fully determined by the length of the velocity-coherent region in the shocked plane along the line of sight. The geometry in the transverse direction in the plane is largely irrelevant; a saturated planar maser can generally be modeled as a disk, and a disk maser observed in the plane appears as bright as an equivalent filamentary maser whose length equals the disk diameter. Of the two independent dimensions perpendicular to the filament axis, one is equal to the disk thickness and the other is somewhat smaller than the size of the disk's unsaturated core. In astrophysical shocks, we show that the last two dimensions are approximately equal, so that the equivalent filament is roughly cylindrical. The ratio of the equivalent filament length to its width, or the effective aspect ratio, is determined by the disk diameter and the pumping scheme. We find effective aspect ratios ($\sim$5–50) that are in agreement with values previously inferred from observed brightness temperatures.

Subject headings: masers — stars: formation

1. INTRODUCTION

H_2O masers are seen in many star-forming regions, and their enormous brightness and small size permits one to study the dynamics of these regions on very small scales. Observations of the radial velocities of these masers suggest that they are of two types, low velocity and high velocity, but proper motion measurements indicate that in fact the two types of maser have the same space velocities (Genzel et al. 1981). These velocities are typically greater than 30 km s^{-1} and can exceed 100 km s^{-1} (Genzel 1986). However, although the kinematics are the same, there are clear differences in intensities between the two populations, with the low-velocity features being much brighter. This then indicates that the angular distribution of the radiation must have a strong directional dependence, peaking in the direction perpendicular to the maser clump velocity. In other words, there are large differences in gains along and across the direction of motion of maser features. These points are well integrated in a model wherein the masers are located behind shock fronts (Elitzur, Hollenbach, & McKee 1989, hereafter EHM). The planar geometry of shocked material provides a natural selection between lines of sight aligned with and perpendicular to the shock velocity. Shocks observed face-on display high radial velocity masers whose gains are limited by the shock thickness, while maser features observed in shocks moving perpendicular to the line of sight have small radial velocities and gains that can be arbitrarily large, in principle; the only limitations on the gains are imposed by the requirement of velocity coherence along the line of sight, unrelated to fundamental shock properties.

The calculations of H_2O maser pumping efficiency in the shock environment were repeated by Neufeld & Melnick (1990, 1991) and Kylafis & Norman (1991, hereafter KN), producing good agreement with the efficiencies presented in EHM. A survey of star-forming regions by Tofani et al. (1991) indicates that H_2O maser luminosities and mechanical energy input from shocks associated with CO outflows are correlated, as expected from our model. Moreover, the EHM calculations predicted the existence of additional maser transitions with photon luminosities comparable to those of the 22 GHz maser. Although detection of these particular lines is beyond current capabilities, other maser transitions among similar levels outside the scheme included in our calculations have since been discovered (Menten, Melnick, & Phillips 1990a; Menten et al. 1990b; Cernicharo et al. 1990), and more have been predicted (Neufeld & Melnick 1991). The larger energy level schemes included in the calculations of Neufeld & Melnick adequately explain the new masers, providing additional support for our basic model for the H_2O masers in star-forming regions.

In our model calculations of brightness temperature (EHM), the masers were assumed to be elongated filaments in shocked slabs, presumably structures that map out gain paths with favorable velocity coherence in a turbulent medium. These cylinders need not be defined by density enhancement; velocity coherence would suffice. The calculations showed that the masers produced by shocks are generally saturated. For optimum shock parameters (preshock density of order 10^7 cm^{-3} and shock velocity of order 40–200 km s^{-1}), EHM showed that the peak brightness temperature observed along the filament axis is given by

$$T_{b,\mathrm{peak}} \simeq 10^{12} a_1^3 \mathrm{K}\ , \tag{1.1}$$

where $a = 10a_1$ is the aspect ratio (length/diameter) of the filament. Aspect ratios of $\sim$10 are required to explain common brightness temperatures ($\sim 10^{12}$ K), with a few filaments

[1] Department of Physics and Astronomy, University of Kentucky, Lexington, KY 40506.
[2] NASA/Ames Research Center, MS 245-3, Moffett Field, CA 94035.
[3] NRC Senior Research Associate.
[4] Departments of Physics and of Astronomy, University of California, Berkeley, CA 94720.

having aspects as large as ~ 50 for occasional extreme brightness temperatures, $\gtrsim 10^{14}$ K. These estimates are supported by the recent line width analysis of Nedoluha & Watson (1991). How such structures might form and what physics controls the velocity coherence remained unspecified. As we show here, these questions and the actual geometry of the velocity coherent region in the plane of the slab in fact have little bearing on the calculated brightness temperatures; i.e., velocity coherent thin disks are equally adequate for producing the observed masers.

2. AMPLIFICATION- AND MATTER-BOUNDED MASERS

For a given pumping scheme, the brightness temperature of an unsaturated maser can be immediately determined from the source's length along the line of sight because the gain, τ, is simply proportional to it; there is no need to even consider the geometrical shape. In a saturated maser, on the other hand, the problem is more involved because the dependence of gain on distance traveled through the source varies between the saturated and unsaturated domains. As a result, the brightness temperature in any given direction cannot be determined before a complete solution of the full maser structure has been attained. This solution is highly dependent on the source geometry; indeed, it cannot even be attempted without fully specifying the geometry.

A convenient approach for solving the problem is obtained by noting that, in all sources with an appreciable gain, whether saturated or not and no matter what their shape, maser radiation is highly beamed (Elitzur 1990b, hereafter E90). At any location in an arbitrarily shaped maser, the longest chord through the source provides an axis that breaks the local symmetry, defining the direction μ_0 of the local dominant ray. From expressions listed in E90 and using the same standard notations, the radiative transfer equation for the intensity $I(\mu_0)$ along the dominant ray is

$$\frac{dI(\mu_0)}{dl} = \frac{h\nu\Phi}{\Omega}\frac{J}{J + J_s} . \tag{2.1}$$

Here Φ is the volume production rate of inverted population, $\Omega = 4\pi J/I(\mu_0)$ is the beaming solid angle, J is the angle-averaged intensity, and J_s is the saturation intensity; specifically, $J_s = \Gamma/2B$, where Γ is the loss rate of the maser system and B is the Einstein B-coefficient of the maser transition. As the first factor on the right-hand side indicates, essentially all the maser photons generated locally are channeled into the beaming angle Ω in the direction of the dominant ray. The second factor, $J/(J + J_s)$, is simply the efficiency with which the maser converts inversion-generating pump events into induced-emission photons, reflecting the only essential difference between unsaturated and saturated operation: when the maser saturates ($J > J_s$), this efficiency becomes unity. As a result, the intensity, i.e., the brightness temperature, of a saturated maser can be easily calculated once the (geometry-dependent) beaming angle has been determined. The brightness is controlled by photon generation inside the beaming cone; material outside the beaming cone has no direct bearing on the brightness of the radiation inside the beaming cone, except in defining the direction of the dominant ray.

Saturated masers with the same length and beaming angle along the line of sight will have the same brightness, irrespective of their global geometry. It is evident, though, that the geometry could play a major role in determining the beaming angle in the first place. We distinguish two types of beaming for saturated masers which we call *amplification-bounded* and *matter-bounded*. Amplification-bounded masers have as their prototype spherical masers (Goldreich & Keeley 1972; E90) and are characterized by observed sizes significantly smaller than their projected physical size. As evident from Figure 1, a given observer sees the highest intensities from those points on the surface whose beaming cones ($\Omega = \pi\theta^2$) contain the observer's direction. The intensity falls off significantly when the observer lies on the edge of the radially directed beaming cone. This determines the observed area of a spherical maser, $A_{obs} = l^2\Omega$; it is a small circular area whose radius is $R_l = l\theta = (A_{obs}/\pi)^{1/2}$. Figure 2a displays the beaming pattern and observed radius of a saturated spherical maser. The beaming pattern is controlled by passage through the unsaturated core, where the amplification varies exponentially with distance.

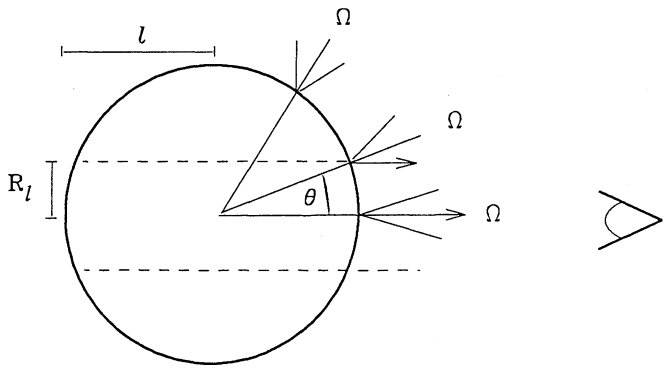

FIG. 1.—Beaming solid angle (Ω) and observed size (R_l) of a spherical maser, and the equivalent cylindrical maser (*dotted lines*).

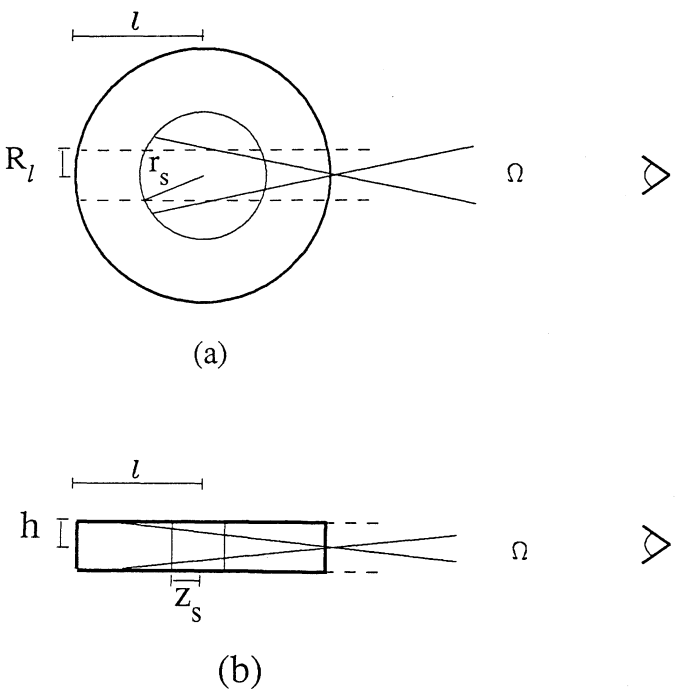

FIG. 2.—Beaming in saturated masers with (*a*) spherical and (*b*) cylindrical shapes. In (*a*) R_l is the observed size and r_s is the radius of the unsaturated core. In (*b*), the observed size is h and the half-length of the unsaturated core is z_s.

TABLE 1

MASER PROPERTIES[a]

Property (1)	Sphere (2)	Disk (3)	Cylinder (4)
1. Ω, unsaturated	$\frac{\pi}{\kappa_0 l}$	$\left(\frac{\pi}{\kappa_0 l}\right)^{1/2}\frac{h}{l}$	$\frac{\pi}{4}\frac{h^2}{l^2}$
2. A_{obs}, unsaturated	$\frac{4\pi l^2}{\kappa_0 l}$	$\frac{4\pi^{1/2} lh}{(\kappa_0 l)^{1/2}}$	πh^2
3. Saturation condition	$\frac{e^{2\kappa_0 l}}{2\kappa_0 l} = 2\gamma$	$\frac{e^{2\kappa_0 l}}{(2\kappa_0 l)^{3/2}} = \frac{(2\pi)^{1/2}\gamma}{\kappa_0 h}$	$\frac{e^{2\kappa_0 l}}{(2\kappa_0 l)^2} = \frac{4\gamma}{(\kappa_0 h)^2}$
4. Core size equation[b]	$\frac{e^{2\kappa_0 r_s}}{(2\kappa_0 r_s)^3} = \frac{6\gamma}{(\kappa_0 l)^4}$	$\frac{e^{2\kappa_0 r_s}}{(2\kappa_0 r_s)^{3/2}} = \frac{2(2\pi)^{1/2}\gamma}{(\kappa_0 l)^2\kappa_0 h}$	$e^{2\kappa_0 z_s} = \frac{3\gamma}{(\kappa_0 h)^2}$
5. Ω, saturated	$\frac{\pi}{\kappa_0 r_s}\frac{r_s^2}{l^2}$	$\left(\frac{\pi}{\kappa_0 r_s}\right)^{1/2}\frac{r_s h}{l^2}$	$\frac{4\pi}{11}\frac{h^2}{l^2}$
6. A_{obs}, saturated	$\frac{\pi r_s^2}{\kappa_0 r_s}$	$\frac{2\pi^{1/2} r_s h}{(\kappa_0 r_s)^{1/2}}$	πh^2
7. $J(l)$, saturated	$\frac{1}{3} J_s \kappa_0 l$	$\frac{1}{2} J_s \kappa_0 l$	$\frac{7}{12} J_s \kappa_0 l$
8. $I(l, \mu = 1)$, saturated	$\frac{4}{3} J_s \kappa_0 l^3 \frac{\kappa_0 r_s}{r_s^2}$	$2\pi^{1/2} J_s \kappa_0 l^3 \frac{(\kappa_0 r_s)^{1/2}}{r_s h}$	$\frac{77}{12} J_s \kappa_0 l^3 \frac{1}{h^2}$
9. kT_b, saturated	$\frac{1}{3}\left(\frac{hc^2}{\nu}\right)\Phi l^3 \frac{\kappa_0 r_s}{r_s^2}$	$\frac{\pi^{1/2}}{2}\left(\frac{hc^2}{\nu}\right)\Phi l^3 \frac{(\kappa_0 r_s)^{1/2}}{r_s h}$	$\frac{77}{48}\left(\frac{hc^2}{\nu}\right)\Phi l^3 \frac{1}{h^2}$
10. L_{iso}/L, saturated	1	$2\frac{l}{h}$	$\frac{77}{24}\frac{l^2}{h^2}$
11. Core saturation	$(\kappa_0 l)^4 = 6.55\gamma$	$(\kappa_0 l)^2 \kappa_0 h = 1.37\gamma$	$(\kappa_0 h)^2 = 0.75\gamma$
12. Core size equation[c]	$r_c^4 = \frac{l^4}{6\gamma}$	$r_c^3 = \frac{l^2 h}{\gamma}$	$z_c^2 = \frac{4h^2}{3\gamma}$

[a] Comparison of masers with identical, and uniform, physical properties (unsaturated absorption coefficient κ_0, saturation intensity J_s, and source function $S = J_s/\gamma$) but different geometrical shapes: col. (2) spherical masers with radius l; col. (3) disk masers with radius l and half-height h; and col. (4) cylindrical masers with half-length l and radius h. The aspect ratios l/h of the disks and cylinders are assumed to obey the filamentary condition, eq. (2.2). The core size equations determine the sizes of unsaturated[b] and saturated[c] cores. In these equations, r_s is the unsaturated core radius of spheres and disks, and z_s is the core half-length in a cylinder. Similarly, $r_c(z_c)$ is the radius (half-length) of a saturated core. L_{iso} is the maser's isotropic luminosity determined from the observed flux, measured in the plane of the disk and along the axis of the cylinder, while L is its actual overall luminosity.

Since the size r_s of the unsaturated core is determined by l, the beaming angle is determined by the size of the sphere. The outside observer sees much higher intensities for rays which pass through the unsaturated core, therefore the observed size $R_l < r_s$ can be much smaller than the physical size l. We call such masers "amplification-bounded" because the amplification process controls the observed size. Column (2) of Table 1[5] summarizes the properties of spherical masers of radius l; $\kappa_0 = \Phi h\nu/4\pi J_s$ is the unsaturated absorption coefficient.

Matter-bounded masers have as their prototype the filamentary maser (Goldreich & Keeley 1972; Elitzur, McKee, & Hollenbach 1990, hereafter EMH), and are characterized by observed sizes equal to their projected physical size. Column (4) of Table 1 summarizes the properties of cylindrical masers.

[5] Note that for some quantities, the table provides only implicit expressions of the form $x^{-n}e^x = b$, where b and n are constants. This equation has a solution only if $b \geq e$. There are two branches to the solution, $x > n$, which is the relevant one, and $x < n$. An approximate solution for the first branch, accurate to within about 3%, is $x \simeq \ln(n^n b) + n[2\ln\ln(n^n b)^{1/n}]^{1/2}$.

For a radius h and half-length l, the aspect ratio $a = l/h$ is assumed to obey the filamentary condition

$$l/h \gg \max[1, \kappa_0 h/4] \qquad (2.2)$$

(EHM). This condition ensures that the beaming angle along the axis of an unsaturated filament is equal to the cap solid angle $\pi/4a^2$, and is smaller than the intrinsic radiation beaming angle of an unsaturated sphere with radius l. In saturated filaments, the unsaturated core extends to their outer radius and has radius h and half-length z_s (see Fig. 2*b*). The beaming angle is unrelated to the unsaturated core dimension z_s. Instead, as in an unsaturated filament, the beaming is controlled by the cap solid angle, although the beaming solid angle is somewhat larger, and the observed size is h. We term such masers "matter-bounded" because the beaming, and the observed size, are fully controlled by the matter distribution. Note that a saturated maser can be matter-bounded either because the masing molecules are confined to a sufficiently thin region, as in a shock, or because velocity gradients are sufficiently large

that molecules with the correct radial velocity to emit at the observed frequency are so confined.

From the discussion of § 5 in EMH it follows that models that produce the same brightness temperature, T_b, and observed area, A_{obs}, are indistinguishable by maser observations because these are the only quantities that can be determined unambiguously. Now, from any given direction a spherical maser appears as a small circular area (see Fig. 1) whose radius is R_l; entries 2 and 6 in column (2) of the table provide the relevant expressions for unsaturated and saturated spheres, respectively. A spherical maser therefore appears identical (to within factors of order unity) to the cylindrical masers outlined with dashed lines in Figures 1 and 2, as both structures share the same observable properties in the indicated direction. Therefore, a spherical maser with radius l uniquely defines an equivalent cylindrical maser with half-length l and radius R_l. As a result, for a given pumping scheme, each length scale l determines a characteristic aspect ratio

$$a_l = \frac{l}{R_l} = \frac{l}{(A_{obs}/\pi)^{1/2}} . \tag{2.3}$$

Note that although each sphere corresponds to a cylinder, the converse is not true: for a given set of microphysical parameters, cylinders of a specified half-length l can exhibit a range of brightnesses I as the aspect ratio is varied (matter-bounded beaming), whereas the brightness of a sphere of that radius is determined (amplification-bounded beaming).

Figure 3 displays the properties of the cylinders equivalent to spherical masers when the pump scheme is characterized by $\gamma = 10^6$, a typical value for the ratio of J_s to the source function S in astronomical masers (see Elitzur 1990a). The bottom panel displays the variation with sphere radius l of the equivalent-cylinder radius R_l; both quantities are expressed in terms of the natural length scale $1/\kappa_0$. The top panel displays the corresponding effective aspect ratio a_l. As long as the sphere is unsaturated, R_l increases as $l^{1/2}$ (eq. [2] in the table) and hence a_l increases as $l^{1/2}$ too. Saturation (indicated in Fig. 3) of the outer shell of a spherical maser occurs when $\kappa_0 l = 8.7$, as can be determined from equation (3) in the table. With further increase in radius, the sphere enters the parameter regime of saturated operation, the saturated shell thickens, and the maser's observed size is determined by the unsaturated core. The core radius r_s is determined from equation (4) in the table, and it slowly *decreases* now with increase in overall radius l. With it, the maser's observed radius R_l (eq. [6] in the table) is slowly decreasing (roughly logarithmically) with l, as displayed by the figure. The corresponding aspect ratio *increases* with l, slightly faster than linearly; note the great disparity in the scales of the vertical axes of the two panels. The abruptness of the transition to saturation reflects the approximations assumed for the saturated solution (the overall radius is assumed to be much larger than the core radius); it is of little significance, as evident from the behavior of the aspect ratio a_l. The saturated portion of the figure is the one with greatest significance to astronomical masers, as the aspect ratios closely correspond to values required to produce the brightness temperatures of observed masers. A saturated sphere with radius l and an equivalent, independent cylinder aligned along the line of sight are virtually identical for the same volume-uniform pump and loss rates. As shown in EMH, apart from numerical factors of order unity, the two configurations are indistinguishable, as they share the same observed area and nearly identical beaming angles, hence brightness temperatures (as is also evident from the expressions for the intensity and brightness temperature along the dominant ray, entries 8 and 9 in the table).

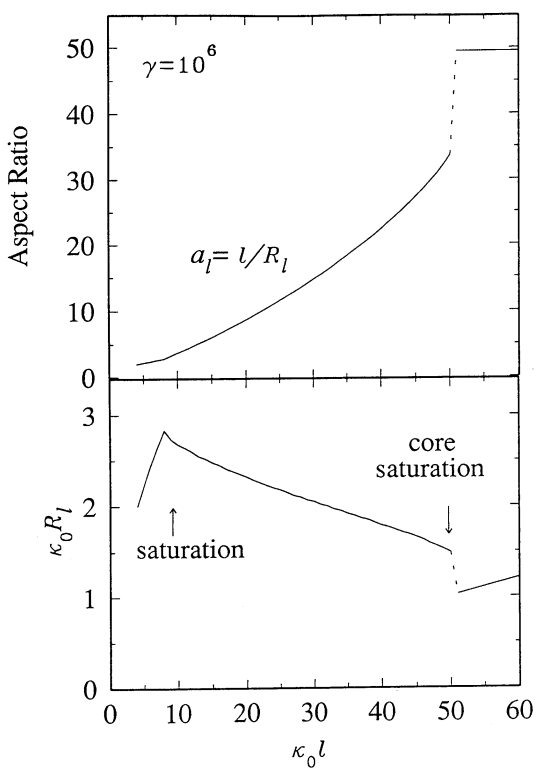

FIG. 3.—Properties of cylindrical masers equivalent to spherical masers of radius l when the pumping scheme is characterized by $\gamma = 10^6$, a typical value for the ratio of the saturation intensity J_s to the source function S in astronomical masers.

With further increase in radius, the core finally saturates when the sphere's radius obeys $\kappa_0 l = 50.6$ (Table 1, eq. [11]) and the maser is now fully saturated. Subsequently, the core radius (now equal to the observed radius) increases in proportion to the overall radius (Table 1, eq. [12]) and the aspect ratio saturates at a maximum value of 49.5. The discontinuity in the figure reflects the shortcomings of current theory. Steady-state solutions have been developed for the two regimes corresponding to unsaturated and saturated cores but the transition between the two has not yet been studied in the literature. Formally, the transition to core saturation requires that the unsaturated core first disappear (hence $R_l \to 0$ and $a_l \to \infty$) before the source settles into the steady-state solution with a saturated core.

A fundamental result emerges from these figures: *Every spherical maser, the quintessential amplification-bounded source, defines an equivalent matter-bounded filamentary maser structure.* From any given direction, the appearance of a spherical maser is indistinguishable from that of the equivalent cylindrical maser. Obviously, if the sphere was deformed outside the cylindrical volume outlined in Figures 1 and 2, the properties observed in the indicated direction would not change substantially; as just shown, we can even entirely remove all the excess material without any appreciable effect on observed properties. Although such removal will affect the core dimensions, thus the beaming angle, the corresponding changes are only logarithmic. Apart from such logarithmic factors, the brightness tem-

perature and observed size of an amplification-bounded maser source are essentially fully determined by the magnitude of the gain along the dominant ray in the line of sight and are independent of the geometry outside the corresponding beaming cone. Equivalently, a given path length along the line of sight defines a characteristic aspect ratio a_l (eq. [2.2]), which can be unambiguously associated with it. The source shape in the transverse direction is largely irrelevant as long as we do not consider structures so narrow that they become filamentary with an actual aspect ratio $a = l/h$ exceeding the characteristic aspect ratio $a_l = l/R_l$.

3. DISK MASERS

Just as spheres are an idealization of amplification-bounded masers and cylinders are of matter-bounded ones, so disks represent an idealization of masers that are amplification-bounded in one direction (the plane of the disk) and matter-bounded in the perpendicular direction. The symmetry of the disk permits analytic calculations of its brightness, but, as in the case of the sphere, deviations from circular symmetry outside the beaming cone should not significantly affect the emission inside the cone. As the prototype of the planar maser, the disk also represents masers associated with shocks.

Disks are intermediate between spheres and cylinders, partly matter-bounded and partly amplification-bounded. Column (3) of Table 1 presents the properties of disk masers with radius l and half-height h, assumed to obey the filamentary condition, eq. (2.2). This ensures that beaming orthogonal to the plane is matter-bounded and is controlled by the angle h/l, while beaming in the plane is amplification-bounded and is governed by an angle θ. For spherical masers, the beaming solid angle is $\Omega = \pi\theta^2$; for a disk, it is $\Omega = (h/l)(2\theta)$. In saturated disks, the relevant case in practice, calculation of the growth of I through the unsaturated core shows that θ, which is proportional to J/I, is given by

$$\theta = \frac{1}{2I(0)} \int I(\theta)\, d\theta = \frac{r_s}{2l} \left(\frac{\pi}{\kappa_0 r_s} \right)^{1/2} . \tag{3.1}$$

The various expressions in the table were derived using the techniques developed in E90 and EMH. Matter-bounded beaming orthogonal to the plane was handled in lowest order of the expansion introduced in EMH, which provides sufficient accuracy for the present discussion. In this lowest order treatment, emission emerging from the sides of the disk is ignored. In the case of the cylinder, inclusion of this emission to first order increases the beaming solid angle by a factor 16/11, and the tabulated results for the cylinder include this first-order correction. The correction in disk masers, where it only applies along one axis, can be expected to be even less significant. As could be expected, disks provide the transition from spheres, listed in column (2), to cylindrical masers with radius h and half-length l, listed in column (4). Both the functional forms and numerical coefficients of the various expressions display a clear sequence. The only significant difference between the three geometries is the increasing disparity between the observable L_{iso}, the isotropic luminosity, and L, the actual luminosity, which is unobservable.

When a saturated disk maser is observed edge-on it will extend a distance $2R_l = 2l\theta$ in the disk plane (see Fig. 4), where θ is given in equation (3.1). Since the maser is matter-bounded in the perpendicular direction, it will have a thickness $2h$ in that direction. If the disk is too thick, it will become

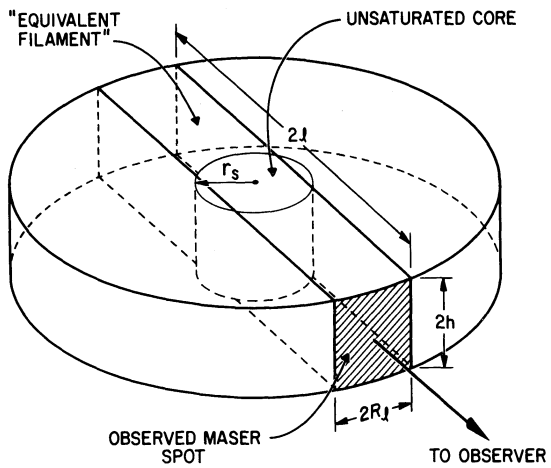

FIG. 4.—A saturated disk maser of thickness $2h$ and radius l contains an unsaturated core of the same thickness and a radius r_s. The maser radiation is beamed radially in the plane of the disk to the observer, who sees a maser spot of height $2h$ and width $2R_l < 2r_s$. The observed properties of the maser are equivalent to those of a filamentary maser of length $2l$, height $2h$, and width $2R_l$. For the shock models of EHM, $R_l/h \sim 0.5$ so that the filament is almost cylindrical.

amplification-bounded in the normal direction and behave like a sphere instead of a disk. We can estimate the maximum disk thickness set by the condition that it remain matter-bounded normal to the shock plane by treating the unsaturated core of the maser as a cylinder oriented in the normal direction with length $2h$ and radius r_s, and then demanding that this cylinder be unsaturated as well (see eq. [3] in Table 1). For a typical value of $\gamma = 10^6$, we find that the core remains unsaturated in the normal direction for $\kappa_0 h < (8.6, 10)$ if the aspect ratio $a = l/h = (1, 30)$. (Note that the value of $\kappa_0 h$ for which a maser with unit aspect ratio saturates is almost the same as the value $\kappa_0 l = 8.7$ at which a sphere saturates.) This value of $\kappa_0 h$ is comfortably greater than the value $\kappa_0 h = 3.9$ characterizing the shock models of EHM, so we conclude that such models are indeed disklike. The observed area of an edge-on disk maser is $A_{obs} = 4R_l h$, which is evaluated in entry 6 of Table 1.

The observed *shape* of the maser is determined by the ratio R_l/h. For the shock models of EHM, this ratio varies slowly from about 0.62 to 0.44 as the aspect ratio l/h varies from 1 to 30; in other words, the maser spots are roughly round, with a modest elongation in this case that is normal to the plane of the disk. Current observational resolutions do not yet permit precise shape determinations of maser spots in the plane of the sky, although such information may become available with the advent of the VLBA and space VLBI.

4. DISCUSSION

As evident from the table, for the same uniform physical properties and line-of-sight characteristic dimension l, all three geometries roughly share the same maser characteristics when $h \simeq r_s$ and $\kappa_0 r_s$ is of order unity. However, while the maser properties are essentially geometry independent, inversion properties are not. The radius l of a spherical maser is always limited because loss lines of the pump cycle become optically thick for sufficiently large spheres, and the maser thermalizes. In contrast, there are no similar limitations on the size l of either disks or filaments. In both cases thermal photons can escape along the short dimension h, and l can increase arbi-

trarily without any effect on the basic inversion efficiency of the pumping scheme throughout the source. In other words, brightness temperatures of amplification-bounded masers are always limited, whereas those that are matter-bounded in at least one dimension are not. Therefore, for all practical purposes, the pumping scheme and the maser length fully determine the brightness temperature of planar masers: *for a given thickness, all planar masers with the same length along the line of sight have essentially the same brightness temperature, irrespective of their geometrical shape.*

We propose that the main ingredient in generating the high brightness temperatures of H_2O masers in star-forming regions is the planar geometry of the shocks that produce them. This then explains why these masers are so much brighter than their counterparts in late-type stars even though the density, temperature, H_2O abundance, and pumping schemes are rather similar in both cases (cf. Cooke & Elitzur 1985). The reason for this disparity is that large inverted columns cannot be generated in the ordered flows of stellar winds where the maser geometry is in general fully three-dimensional and amplification-bounded. Occasional observations of high brightness hot spots probably reflect chance velocity coherence along the line of sight resulting from the superposition of turbulent motions on the ordered wind flow. In contrast, the slab geometry of shocked material in star-forming regions generates an inverted environment with, in principle, unrestricted maser lengths in the slab plane. Maser lengths, and brightness temperatures, are limited only by velocity coherence or by the extent to which the planar geometry holds. The geometry in the transverse direction in the plane is largely irrelevant.

Shocks in star-forming regions can be either J-type shocks or C-type shocks (Draine 1981), which are generally dissociative or nondissociative, respectively. Our shock-model calculations of H_2O masers in star-forming regions (EHM) were for shocks sufficiently fast that the H_2 is initially completely dissociated (J-type), but reforms downstream and produces a warm ($T \sim 400$ K) slab of H_2O–rich gas. C-type shocks also produce large regions of hot H_2O, but calculations of the maser emission from such shocks have yet to be carried out. Our calculations show that for a prototype maser slab, with $n(H_2) = 10^9$ cm^{-3}, $[H_2O]/[H_2] = 6 \times 10^{-4}$, $T = 400$ K, and $2h = 10^{13}$ cm, the factor $\kappa_0 h = 3.9$. As shown in § 3 above and as can be confirmed from Figure 3, this value is similar to the value of $\kappa_0 R_l$ for amplification-bounded saturated masers for $\gamma = 10^6$, which the model calculations show is the appropriate value for the H_2O neutral-collisions pumping scheme. The two characteristic maser dimensions in the plane of the sky (the apparent radius and the half-height) are thus nearly the same for all relevant lengths l. Therefore, to a good degree of accuracy, Figure 3 is applicable to disk configurations as is. Since a disk radius (maser length) uniquely determines an aspect ratio, the analysis of phenomenological H_2O maser properties presented in EHM remains essentially intact and the aspect ratios we derived from brightness temperatures find a simple explanation. Observations show that brightness temperatures usually span the range $\sim 10^{11}$–10^{14} K (Genzel et al. 1981; Genzel 1986). Since T_b varies in proportion to l^3, maser lengths generally vary by about factor 10 in any given source.

An alternative view for the beaming of masers has been presented by KN, who considered a model in which the beaming is due to velocity gradients, with a relatively small gradient in the beaming direction and a large one normal to that direction. They adopted the Sobolev approximation and showed that for unsaturated masers, velocity gradients provide relatively poor beaming: If the size of the velocity coherent region along the line of sight is l_v and that normal to the line of sight is h_v, then the beaming angle Ω is of order h_v/l_v rather than the value $(h_v/l_v)^2$ expected for a filament with an aspect ratio l_v/h_v. This result, which is consistent with previous studies by Elitzur, Goldreich, & Scoville (1976) and by Deguchi (1982), corresponds to an amplification-bounded maser in which the velocity gradients cause the region that can interact with a given molecule at a given frequency to be shaped more like a cone than a filament. In shocks, the shape of the masing region, in one direction at least, is controlled primarily by the shock temperature and chemistry; in J-shocks, velocity gradients normal to the plane of the shock are not important. The argument of KN will be valid in the plane of the shock provided that the maser is unsaturated, and that the size of the masing region is set by a linear velocity gradient and not by the curvature of the plane of the shock or by higher order velocity gradients. At any rate, the beaming angle is irrelevant to the brightness temperature of an unsaturated maser, which is completely determined by the length along the line of sight irrespective of the geometry.

Once the maser saturates, the Sobolev approximation breaks down, since it is based on the assumption that the medium is homogeneous over a thermal velocity width (Mihalas 1978, p. 471 ff.); in particular, the absorption coefficient at a fixed frequency must be constant in such a region. However, a saturated maser is intrinsically inhomogeneous since in such a maser the absorption coefficient depends on the mean intensity (see eq. [2.1]). We note that beaming angles, and brightness temperatures, have never been properly calculated for saturated masers in the Sobolev approximation. Calculations of the structure of saturated masers in large-velocity gradients have yet to be made, but they should be qualitatively consistent with the results we have found: the beaming is determined by the size of the unsaturated core, not by the angular size of the region of velocity coherence. Note that the disk model we have considered has a region of velocity coherence extending over 2π radians in the plane of the disk, much greater than that in the KN model. The beaming from the unsaturated core leads to a high maser brightness temperature over the entire 2π radians, giving a high luminosity. We have assumed that the velocity gradient is small over the size of the unsaturated core, $dv/dl < v_{\rm th}/r_s$; violation of this condition will tend to reduce the maser luminosity rather than the peak maser brightness.

As an alternative to the smooth velocity field considered by KN, one might model the flow behind a shock as a turbulent flow in which the size of a velocity coherent region, or cell, is determined by higher order velocity derivatives. These cells may be visualized as planar structures that are not highly elongated—in other words, they may be idealized as disks. Each cell then corresponds to a single maser that can be analyzed with the disk model presented in the previous section, and the distribution of cell radii characterizes the distribution of maser lengths in the plane of the shocked slab. Large gains (high brightness temperatures) can occur when either a single cell has a large radius (amplification-bounded planar maser) or, similar to the proposal by Deguchi & Watson (1989) of filament alignment, two or more small cells happen to be aligned (amplification-bounded masers mutually aligned to produce matter-bounded beaming). Obviously, both cases may occur in every source, and which contribution dominates at a

given brightness temperature depends on the distribution of cell radii.

The foregoing discussion shows that the maser geometry is not directly observable. Two methods exist to distinguish between amplification-bounded and matter-bounded geometries. The first one involves separation between maser spots. In matter-bounded masers the apparent and real radii in the plane of the sky are the same, while in amplification-bounded masers the apparent radius is much smaller than the physical dimension. Therefore, the detection of a number of features spaced at intervals of order their size implies matter-bounded beaming (except in the unlikely case that the centers of the masers happen to be aligned along the line of sight). If the closely spaced maser spots are irregularly arranged in the plane of the sky, then they must be filamentary; if the closely spaced spots are roughly collinear, then the masers could be disk-shaped. However, a large separation between features does not allow any conclusions about the geometry.

A more direct observational test involves the frequency dependence of the beaming angle Ω (see E90, EMH). While matter-bounded beaming is frequency-independent, in amplification-bounded masers the beaming angle varies with frequency, and with it the observed transverse dimension (as long as the core does not saturate). In the standard theory of astrophysical masers (e.g., Litvak 1970; Goldreich, Keeley, & Kwan 1973; Goldreich & Kwan 1974), the radiation is assumed to be described by plane waves and the intensity at one frequency is completely uncoupled from that at other frequencies. In this case, the results in Table 1 apply at each frequency, and one can generalize κ_0, r_s, and z_s to $\kappa_{0\nu}$, $r_{s\nu}$, and $z_{s\nu}$, respectively. This generalization of the results in Table 1 shows that the observed size of a filamentary maser is fixed, while for an amplification-bounded maser it varies with frequency shift from line center. For a disk maser, if we approximate $\kappa_{0\nu} r_{s\nu}$ as being independent of frequency (a reasonably good assumption), and if we assume that the size of the maser is independent of frequency (a questionable assumption, since it depends on the unknown velocity structure of the maser), then the observed area would scale as $A_{\rm obs} \propto \kappa_{0\nu}^{-1} \propto I_\nu^{-1/2}$. Such an effect has not been observed to date: Genzel et al. (1981) report that observed sizes of individual maser spots in W51 M are roughly constant across the profile, and similar results were obtained for a number of sources by Walker & Moran (1990). Note, however, that the shape of the maser spots (and therefore the true brightness temperature) has yet to be measured. The discussion in § 3 indicates that the greater of the two maser dimensions in the plane of the sky is often determined by the disk thickness, which is independent of frequency. Observations of the minor diameter of the maser spots as a function of frequency are required to test the predicted variation of size with frequency.

The theoretical basis of this relation between the frequency and the size has been questioned by the referee, D. Neufeld, who has raised doubts concerning the assumption that different frequencies are in fact independent when one allows for the finite size of the beam. A correct treatment of multidimensional saturated masers is therefore required to determine the line profiles and the frequency dependence of the maser spot size $A_{\rm obs}(\nu)$, which is beyond the scope of this paper. However, the effect of frequency coupling should be greatest in the line wings and we expect that the results in Table 1 will remain valid near line center.

In summary, the planar geometry of H_2O masers in star-forming regions provides a natural explanation for the high brightness temperatures that are observed. These brightness temperatures are controlled by the length of the velocity coherent region along the line of sight; the geometry in the transverse direction in the plane is less important (i.e., filaments are not required). Observations of the size and shapes of maser spots are potentially extremely promising: observations of low-velocity masers can determine the shock thickness $2h$ (the dimensions in the direction of the proper motion) and the apparent diameter $2R_l$, whereas observations of the high-velocity masers can determine the properties of the masers when observed at angles outside the plane of the disk. If such observations confirm the shock model, they will permit detailed analysis of the geometry and microphysics of the masers, providing new insights into the conditions in regions of star formation.

We thank the referee, D. Neufeld, for his useful comments. This work was supported in part by NSF grants AST-9016810 (M. E.) and AST-89-18573 (C. F. M.), and by NASA grant 399-20-01-35 (D. J. H.).

REFERENCES

Cernicharo, J., Thum, C., Hein, H., John, D., Garcia, P., & Mattioco, F. 1990, A&A, 231, L15
Cooke, B., & Elitzur, M. 1985, ApJ, 295, 175
Deguchi, S. 1982, ApJ, 259, 634
Deguchi, S., & Watson, W. D. 1989, ApJ, 340, L17
Draine, B. T. 1981, ApJ, 241, 1021
Elitzur, M. 1990a, ApJ, 363, 628
———. 1990b, ApJ, 363, 638 (E90)
Elitzur, M., Goldreich, P., & Scoville, N. 1976, ApJ, 205, 384
Elitzur, M., Hollenbach, D. J., & McKee, C. F. 1989, ApJ, 346, 983 (EHM)
Elitzur, M., McKee, C. F., & Hollenbach, D. J. 1991, ApJ, 367, 333 (EMH)
Genzel, R. 1986, in Masers, Molecules and Mass Outflows in Star Forming Regions, ed. A. D. Haschick (Westford, MA: Haystack Observatory), 233
Genzel, R., et al. 1981, ApJ, 247, 1039
Goldreich, P., & Keeley, D. A. 1972, ApJ, 174, 517
Goldreich, P., & Kwan, J. 1974, ApJ, 190, 27
Goldreich, P., Keeley, D. A., & Kwan, J. Y. 1973, ApJ, 179, 111
Kylafis, N. D., & Norman, C. A. 1991, ApJ, 373, 525 (KN)
Litvak, M. M. 1970, Phys. Rev. A, 2, 2107
Menten, K. M., Melnick, G. J., & Phillips, T. G. 1990a, ApJ, 350, L41
Menten, K. M., Melnick, G. J., Phillips, T. G., & Neufeld, D. A. 1990b, ApJ, 363, L27
Mihalas, D. 1978, Stellar Atmospheres (2d ed.; San Francisco: Freeman)
Nedoluha, G. E., & Watson, W. D. 1991, ApJ, 367, L63
Neufeld, D. A., & Melnick, G. J. 1990, ApJ, 352, L9
———. 1991, ApJ, 368, 215
Tofani, G., et al. 1991, in Skylines: Proceedings of the third Haystack Conference, ed. A. D. Haschick & P. T. P. Ho (San Francisco: ASP), 89
Walker, R. C., & Moran, J. M. 1990, private communication